



Relationship between summer extreme precipitation anomaly in Central Asia and surface sensible heat variation on the Central-Eastern Tibetan Plateau

Hui Wang¹ · Jie Zhang¹ · Lian Chen² · Dongliang Li¹

Received: 29 May 2021 / Accepted: 8 January 2022 / Published online: 19 January 2022
© The Author(s) 2022

Abstract

In the context of global warming, the frequency and intensity of extreme weather and climate events have increased, especially in Central Asia (CA). In this study, we investigate the characteristics of summer extreme precipitation (SEP) in CA and its relationship with the surface sensible heat (SSH) variation over the central–eastern Tibetan Plateau (CETP). The results suggest that the distribution of SEP in CA is extremely uneven, and the SEP thresholds range from 2 to 32 mm/day, and 80% of them are concentrated in 4–10 mm/day. Both the total amount of SEP and the number of SEP days show significant increasing trends, with the climatic tendencies of 4.4 mm/decade and 0.4 day/decade, respectively. The SSH anomalies over the CETP can affect the SEP and summer drought in CA by regulating the strength of South Asia High (SAH) and the subtropical jet over CA. The strong SSH anomalies over the CETP in late spring (April–May) can be transmitted from the lower to the upper layers through the continuous heating to the atmosphere and lead to the anomalously strong subtropical high over northern Africa and the Arabian Peninsula, the anomalously weak subtropical westerly jet over CA and the anomalously strong SAH in summer. At the same time, the Ural ridge strengthens, the CA trough weakens, and the northern CA is controlled by an anomaly of warm high-pressure ridge. Therefore, the anomaly of water vapor convergence in northern CA weakens. The SEP there will be abnormally less, and the summer drought intensifies. When the SSH over CETP is anomalously weak in late spring, the key circulations are just the opposite. Furthermore, the anomalous water vapor from the Arctic, North Atlantic and western Pacific converges in northern CA and northern Xinjiang, China, which is conducive to the generation of widespread extreme precipitation and the alleviation of summer drought in these regions.

Keywords Tibetan Plateau · Central Asia · Extreme precipitation · Sensible heat flux · Drought

1 Introduction

Central Asia (CA) is a typical arid and semi-arid climatic region located in the Eurasia inland with complex topography, which is also a key region of China's national initiatives of "Silk Road" and "One Belt, One Road". Recently, transboundary cooperation has been increasing between CA

and its neighboring countries. Therefore, the climate change around CA has attracted more and more international attentions (Chen et al. 2016; Peng et al. 2019; Zhu et al. 2020).

CA has obvious climatic variability and fragile ecosystem (Li et al. 2015; Zhang et al. 2016). Previous studies have shown that the temperature in CA rises much faster than the global mean temperature (Chen et al. 2009; Hu et al. 2014). This rapid warming trend has led to significant variation in spatio-temporal patterns of extreme precipitation in CA (Chen et al. 2011; Trenberth et al. 2015; Alexander 2016; Hu et al. 2016; Zhang et al. 2019a). The frequency and intensity of extreme weather and climate events have increased, and the losses caused by meteorological disasters have intensified, seriously affecting the natural ecological environment and the socio-economic sustainable development in the region (Donat et al. 2016; Li et al. 2017; Xenarios et al. 2019; Yu et al. 2019). Therefore, it is of great practical

✉ Hui Wang
wanghui123@nuist.edu.cn

¹ Key Laboratory of Meteorological Disaster, Ministry of Education and Collaborative Innovation Center On Forecast and Evaluation of Meteorological Disasters, Nanjing University of Information Science and Technology, Nanjing 210044, China

² Shanghai Institute of Satellite Engineering, Shanghai 201109, China

significance and scientific value to study the characteristics and causes of the extreme precipitation in CA.

So far, the difficulties in predicting the extreme precipitation in CA are mainly caused by the lack of systematic understanding on its variation patterns and the related atmospheric circulation configurations (Bothe et al. 2012; Li and Wang 2017; Shang et al. 2020). Precipitation-related circulations are vital for addressing these issues. The precipitation in CA is mainly affected by the mid-latitude westerlies, and it is significantly different from the circulation situation in East Asia (EA) which is dominated by monsoon circulations (Schiemann et al. 2009; Liu et al. 2018; Yin et al. 2014; Watanabe and Yamazaki 2014). Previous studies have proved that the precipitation in CA was mainly affected by the strength of the westerly jet stream and the spatio-temporal variations of the North Atlantic Oscillation (NAO) (Aizen et al. 2001; Filippi et al. 2014; Xu et al. 2016; Wei et al. 2017; Liu et al. 2017a; Sun et al. 2019a). In addition, the summer extreme precipitation in CA is closely related to the water vapor transport from the North Atlantic Ocean and the Indian Ocean (Bothe et al. 2012).

The Tibetan Plateau (TP) is located in the southeast of CA. Because of its high mean elevation (over 4 km), huge size (greater than 2.5 million km²) and complex terrain, TP is important in regulating the atmospheric circulation around it (Ye and Wu 1998; Wu and Zhang 1998; Duan and Wu 2005; Zhou et al. 2009; Duan et al. 2011; Ma and Ma 2016; Liu et al. 2017b; Huang et al. 2019; Zhang et al. 2019b; Yu et al. 2021). Many past studies have focused on examining the impact of TP forcing on local climate or on downstream regions of EA and South Asia, but few studies have investigated the impact of TP forcing on the CA climate. A few recent studies have revealed that the thermal conditions of TP can impact the climate variation in upstream regions (Lu et al. 2018; Sun and Liu 2021; Zhang et al. 2021; Liu et al. 2021). For example, Zhang et al. (2021) and Liu et al. (2021) revealed that the variation of TP snow cover is closely related to the summer surface air temperature and precipitation over CA. Sun and Liu (2021) found that the thermal effect of TP controls the summer precipitation in CA and arid EA through the TP-induced compensational downdraft. The surface sensible heat (SSH) over the TP is the dominant source of diabatic heating during the boreal spring (Ye and Gao 1979; Duan et al. 2017). Previous studies have shown that the positive SSH anomaly over the TP generates negative vorticity anomaly at high levels, which influences the atmospheric circulation in the Northern Hemisphere by triggering Rossby wave trains (Wu et al. 2016; Liu et al. 2017b). It is unclear what is the relationship between TP SSH anomalies and the extreme precipitation in CA, and whether the physical mechanisms of thermal influence of the TP on the CA climate are the same as that for the EA

monsoon climate? To this end, this study starts with the variations of SSH over the CETP to investigate the influence of surface thermal anomalies on the summer extreme precipitation (SEP) in CA and the key circulations. We hope this study can provide a theoretical basis for predicting the SEP in CA, and contribute to scientifically reducing the risk of extreme precipitation disasters and ensuring the socio-economic sustainable development.

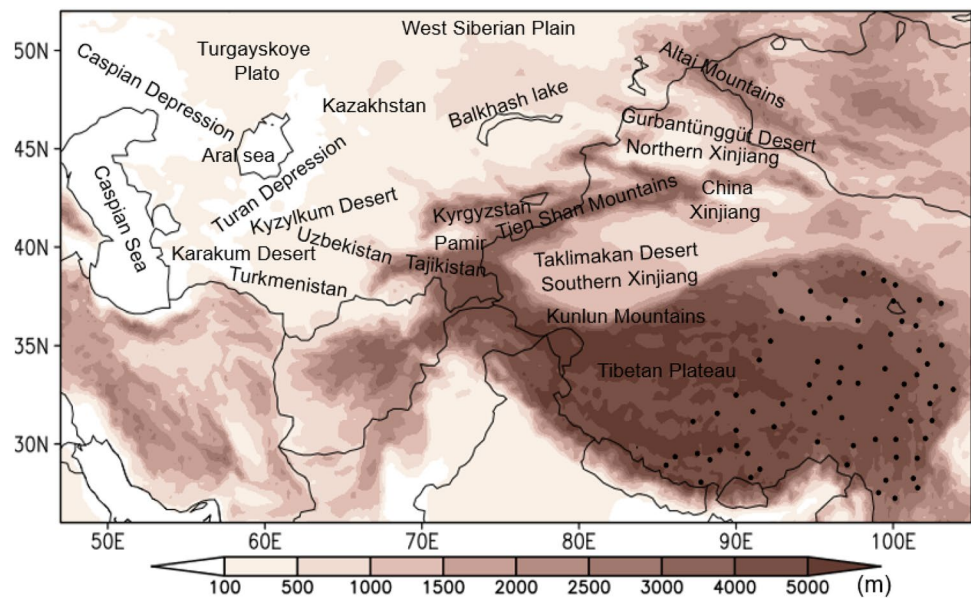
The remainder of this paper is organized as follows. The study area, data and identification method of extreme precipitation are introduced in Sect. 2. The features of SEP in CA are analyzed in Sect. 3. The influences of the SSH variations over the CETP on SEP anomalies in CA, and the key circulation systems are described in Sect. 4 and Sect. 5. Finally, Sect. 6 presents the main conclusions and discussion.

2 Study area, data, and methodology

2.1 Study area

The study area covers five central Asian countries (i.e., Kazakhstan, Kyrgyzstan, Tajikistan, Uzbekistan and Turkmenistan) and Xinjiang Province of China, locates in 48° E–95° E and 35° N–52° N, and has a total area of 5.65 million km² (Fig. 1). CA is located in the hinterland of Eurasia. The southeastern margin of CA is the Pamirs and Tibetan Plateau, with an average elevation of above 4000 m, which is a natural barrier and blocks the warm-moist airflows from the Indian Ocean and the Pacific Ocean (Bothe et al. 2012). CA has a typical temperate desert and grassland climate featured by sharp temperature difference, intensive evaporation, and dry and rainless environments (Li et al. 2015; Zhang et al. 2019a). The geomorphological landscapes of the five countries in CA are mainly deserts, oases and mountains in the south, including the Kyzylkum Desert, the Karakum Desert, the Turan Depression and the Pamirs, and grasslands, plains and hills in the north, including the Caspian Depression, the Turgay Valley and Kazakh Hills. Meanwhile, the geomorphology in Xinjiang is characterized by a basin-range pattern. The Altai Mountains, Tianshan Mountains, and Kunlun Mountains are located in the northern, middle, and southern parts of the region, respectively, and the Junggar Basin and Tarim Basin are located between these mountains (Zhang et al. 2019a). The Tianshan Mountains divide Xinjiang into two regions, southern Xinjiang and northern Xinjiang. Southern Xinjiang is located in the arid desert zone with annual precipitation less than 100 mm, and the Taklimakan Desert, which is the world's second largest mobile desert, is located there. Northern Xinjiang belongs to the mountainous climate, and the annual

Fig. 1 Locations of Central Asia and the meteorological stations on the Central-Eastern Tibetan Plateau



precipitation is about 100–500 mm, mainly concentrating in summer (Wu et al. 2010). The water vapor transported to Northern Xinjiang is mainly from the Atlantic and Arctic Oceans (Zhao et al. 2014).

The data from 70 relatively evenly distributed meteorological stations on the TP are used in this study (as shown in Fig. 1). Because the geomorphological landscapes in the western TP are mostly mountains and deserts, the meteorological stations are mainly concentrated in the CETP.

2.2 Data

The daily precipitation data during 1982–2018 used in this study is from the National Oceanic and Atmospheric Administration (NOAA) Climate Prediction Center (CPC), with a grid spacing of $0.5^\circ \times 0.5^\circ$ (<https://climatedataguide.ucar.edu/climate-data/cpc-unified-gauge-based-analysis-global-daily-precipitation>; Chen et al. 2008). Previous studies have indicated that this dataset has a good performance in CA (Rana et al. 2017).

The monthly gridded global Palmer Drought Severity Index (PDSI) data during 1982–2014 is from the National Center for Atmospheric Research (NCAR), with a grid spacing of $2.5^\circ \times 2.5^\circ$ (<https://psl.noaa.gov/data/gridded/data.pdsi.html>; Dai et al. 2004). The PDSI uses readily available temperature and precipitation data to estimate relative dryness. It is a standardized index that generally ranges from -10 (dry) to $+10$ (wet). The PDSI has been reasonably successful at quantifying long-term drought. As it uses temperature data and a physical water balance model, it can capture the basic effect of global warming on drought through changes in potential evapotranspiration (Dai et al. 2004).

To calculate SSH flux, the monthly measurements of air temperature at 1.5 m above ground level (a.g.l.) from a sheltered thermometer (T_a), ground surface temperature at 0 cm (T_g , measured by using a thermometer where one half is horizontally exposed above ground, and the other half is horizontally interred), wind speed at 10 m a.g.l. (U), and station surface pressure (P_s) at 70 stations (see Fig. 1) on the CETP during 1982–2018 are used. These data are derived from the Chinese surface historical basic meteorological dataset version 3.0 from China Meteorological Administration (CMA). This dataset meets the standards of World Meteorological Organization (WMO) and comprises observations of 20 variables from more than 2,000 stations, and all the data have been subjected to quality control (Ren et al. 2012).

The Global Inventory Modeling and Mapping Studies (GIMMS) Normalized Difference Vegetation Index (NDVI) dataset (<http://ecocast.arc.nasa.gov/data/pub/gimms/3g/>) is used herein to determine the underlying surface types and estimate the bulk transfer coefficients for heat at the CMA stations on the CETP. It has a 15-day temporal frequency, a $1/12$ -degree spatial resolution and a temporal span from July 1981 to December 2018. A detailed description of this dataset can be found in Zhu et al. (2013). Moreover, the National Centers for Environmental Prediction–Department of Energy (NCEP–DOE) reanalysis data is also used herein to describe the characteristics of atmospheric circulation conditions. The Niño 3.4 index is employed to describe the influence of the El Niño–Southern Oscillation (ENSO) on the relationships between SEP and the summer drought in CA and the SSH over the CETP, which is collected from CPC (<https://www>.

cpc.ncep.noaa.gov/data/indices/-ersst5.nino.mth.91-20.ascii).

2.3 Methods

According to the standards of WMO, the extreme precipitation threshold at each grid point in CA is determined by using the international percentile method. First, the non-precipitation days during 1982–2018 are removed at all the grid points. Then, the daily precipitation data in summer

$$C_h = \begin{cases} -0.0045NDVI^2 + 0.0074NDVI + 0.0021 & \text{when } 0.50 \leq I_{SM} < 1 \\ 0.0062NDVI^2 - 0.0020NDVI + 0.0021 & \text{when } 0.35 \leq I_{SM} < 0.50 \\ 0.0120NDVI^2 - 0.0015NDVI + 0.0029 & \text{when } 0 < I_{SM} < 0.35 \end{cases}, \quad (3)$$

(June–August) of each year are sorted in an ascending order at each grid, and the 37-year average of the 90th percentile is taken as the threshold of extreme precipitation at that grid point. Finally, the number of days with daily precipitation greater than or equal to the threshold of extreme precipitation in summer is taken as the number of SEP days, and the cumulative precipitation on SEP days is the total amount of SEP. This method is widely used in the studies of extreme precipitation events (Bonsal et al. 2001; Xiao et al. 2016).

The bulk transfer method for deriving SSH has been widely utilized in TP-related studies (Yeh 1982; Chen et al. 1985; Ye and Wu 1998; Duan and Wu 2005; Yang et al. 2009, 2011; Duan et al. 2011; Zhu et al. 2017; Wang and Li 2019). The formula is as follows.

$$H = \rho_s c_p C_h U (T_g - T_a), \quad (1)$$

where c_p is the specific heat capacity at a constant pressure ($1004.07 \text{ J kg}^{-1} \text{ K}^{-1}$); C_h is the bulk transfer coefficient for heat; U is the wind speed at 10 m a.g.l. (m/s); T_g is the ground surface temperature (K); T_a is the air temperature (K); ρ_s is the air density (kg m^{-3}):

$$\rho_s = P_s / R_d T_a, \quad (2)$$

where P_s is station pressure (P_a) and R_d is specific gas constant of dry air ($287.05 \text{ J kg}^{-1} \text{ K}^{-1}$).

It is worthy of note that C_h plays a key role in determining SSH flux. Numerous evidences show that the value of C_h varies widely on different land cover classes and in different seasons (Wang and Ma 2011; Wang et al. 2019). Due to the complex topography and harsh environmental conditions, direct observation data from field experiments on the TP are particularly scarce, and the determination of C_h is a very complicated problem (Zhao and Chen 2000; Yang et al. 2011). Thus, in the process of deriving SSH by the bulk transfer method, many researches consider C_h as a constant

value (e.g., 0.004 in TP), without considering its seasonal variations and regional differences (Chen et al. 2019).

Recently, Wang et al. (2019) developed a new parameterization scheme using GIMMS-NDVI dataset and field micro-meteorological observations on the CETP. This parameterization scheme takes into account the different meadow types on the CETP, and results suggest it is capable of reflecting the variations of C_h at the regional scale in four seasons. Therefore, this parameterization scheme is applied to estimate C_h for the CETP in this study. It is as follows:

where I_{SM} is the value of summer (June–September) mean NDVI. When I_{SM} is greater than 0.50, the underlying surface is defined as a long meadow; when I_{SM} is in the range of 0.35–0.50, the underlying surface is defined as a short meadow; when I_{SM} is less than 0.35, the underlying surface is defined as a sparse meadow.

First, the I_{SM} of each CMA station is calculated by using the NDVI dataset to determine the underlying surface type. Then, the monthly values of C_h and SSH fluxes at 70 meteorological stations during the period of 1982–2018 are calculated by Eqs. (3) and (1), respectively. Evidences show that the values of C_h calculated by Eq. (3) range from 0.0025 to 0.0050, with obvious seasonal variations and spatial differences, which are smaller in winter and higher in summer. The values in the southeast are higher than in the central-northern TP. The SSH fluxes calculated by Eq. (1) are consistent with the results of Yang scheme (Yang et al. 2009) in terms of the interannual variation and trend characteristics, which can better represent the climatic characteristics of SSH changes over the CETP (Wang et al. 2019).

The mathematical statistics analysis methods used in this paper include regression, correlation, partial correlation and composite analysis. A five-year high-pass Lanczos filter (Duchon 1979; Sun et al. 2019b; Yu et al. 2021) is applied to these datasets to extract the signals of interannual variability.

3 Features of the SEP in CA

Figure 2 presents the distribution of extreme precipitation thresholds and the proportions of grid points with different thresholds in CA. It shows that the SEP thresholds in CA vary between 2 and 32 mm/day, with significant regional differences. The thresholds are within 4–10 mm/day at 80% of the stations. The larger values are mainly located in the

Fig. 2 **a** The proportions of grid points with different threshold ranges and **b** distribution of summer extreme precipitation (SEP) thresholds (units: mm/day) in CA

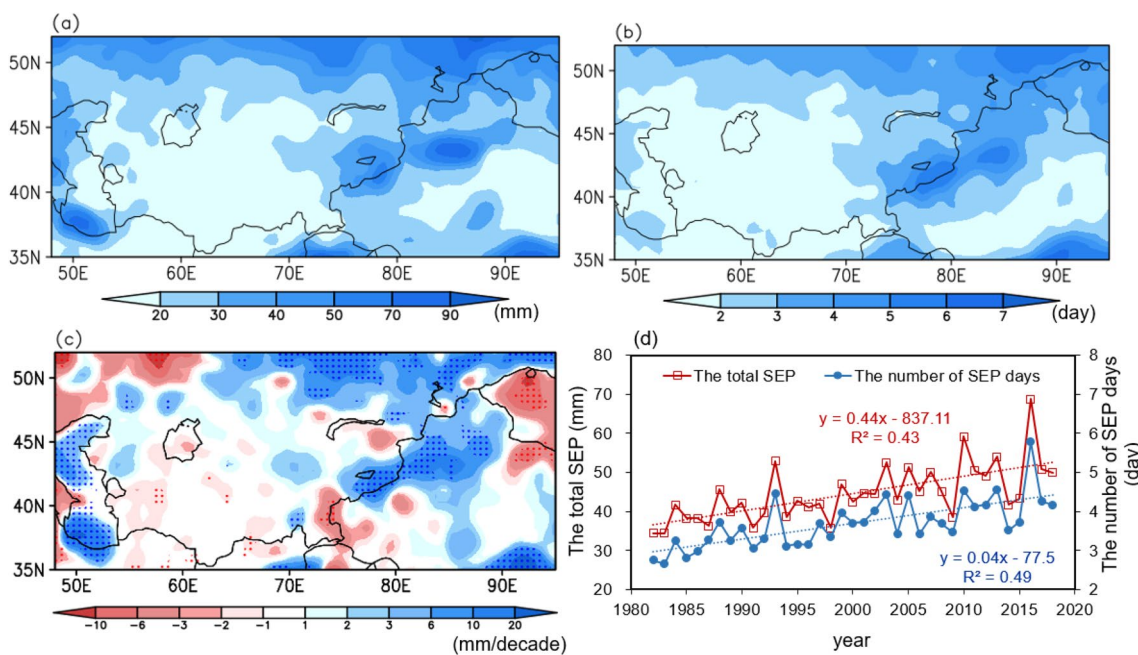
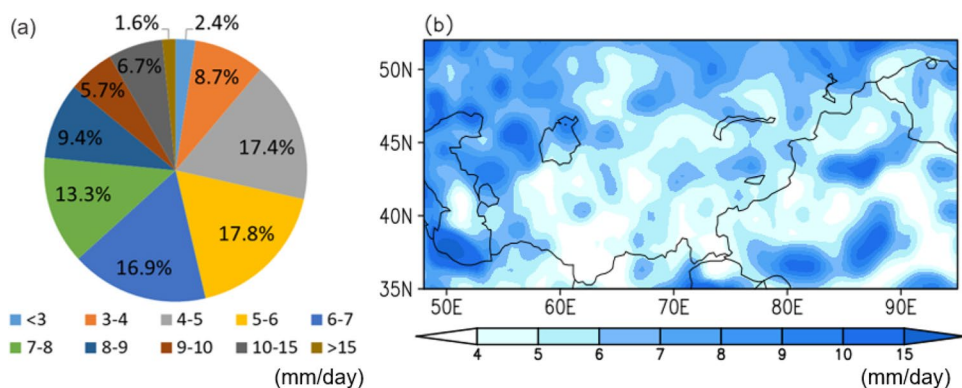


Fig. 3 The spatial distributions of **a** the average total SEP (units: mm), **b** the average number of SEP days (units: day) and **c** the climate tendency rate of total SEP (units: mm/decade) during 1982–2018. **d** The interannual variations of total SEP and the number of SEP days

from 1982 to 2018. The red (blue) solid line is total SEP (the number of SEP days), the red (blue) dotted line, formula and R^2 in **d** are its trend line, linear regression and complex correlation coefficient, respectively

western and northeastern Kazakhstan, especially in the Caspian Depression and West Siberian Plain, and around the Tianshan Mountains in central Xinjiang and the Kunlun Mountains in the south.

The spatial distributions of the average total amount of SEP and the average number of SEP days in CA are shown in Fig. 3a, b, and the two distributions are quite similar to each other. The key areas of SEP are in the northern CA and the Tianshan Mountains, with the average SEP days being about 7 days and the total amount of precipitation being over 90 mm. Central and southern CA has less extreme precipitation in summer, with the total amount of extreme precipitation less than 20 mm and the extreme precipitation days less than 2 days.

The spatial distribution of climate tendency rates of the total amount of SEP in CA is shown in Fig. 3c, it shows that the total amount of SEP has an increasing trend in most areas of CA. 24.8% of the stations are with the increasing rate more than 5 mm/decade, and only 3.8% of the stations have a significant decreasing trend. The regional average climate tendency rate is 4.4 mm/decade (Fig. 3d), passing the t-test at a 99% confidence level (i.e., $P < 0.01$). It also confirms the previous finding that most Asian drylands have been experiencing warm and wet conditions since the 1980s (Shi et al. 2007). The comparisons between Fig. 3c and a show that the regions with a significant increasing trend of extreme precipitation, such as the northeast part of Kazakhstan and the Tianshan Mountains, are consistent with

the areas with more extreme precipitation in Fig. 3a. The central-southern parts of CA with a slightly decreasing trend of extreme precipitation are consistent with the areas with less extreme precipitation in Fig. 3a. This indicates that the increase of SEP in CA mainly occurs in the region with high precipitation. The number of SEP days also shows a significant increasing trend, with the climatic tendency of 0.4 day/decade ($P < 0.01$) (Fig. 3d). This is similar to the findings about extreme precipitation in other regions. For example, the increase and intensification of extreme precipitation have been observed in East Asia, South America, North America and Oceania (Zhai et al. 2005; Pryor et al. 2009; You et al. 2011; Skansi et al. 2013; Ren et al. 2015), which is mainly related to the significant global warming (Xu et al. 2018; Yun et al. 2019). The frequent occurrence and intensification of extreme events caused by the climate warming are becoming a prominent issue in the climate change (IPCC, 2014).

4 Relationship between the SSH over the CETP and the SEP in CA

The influence of the SSH over the TP on the interannual variation of the Asian summer monsoon has been well addressed (Liu et al. 2012, 2017a; Duan et al. 2017; Zhao et al. 2018). There is a significant positive correlation between the intensity of spring–summer TP heat source and summer monsoon precipitation in the Yangtze River valley, and a negative correlation for the summer monsoon precipitation in southern and northern China (Hsu and Liu 2003; Cui et al. 2015). Then, what is the relationship between the SEP in CA and the thermal effect of the TP? What is the key atmospheric circulation system for this relationship? A diagnostic analysis of their relationship will be performed to clarify this issue. The correlation coefficients between the regional average SSH in different periods from April to July over the CETP and the SEP in CA are calculated (Table 1). It is shown that there are stable and significant

negative correlations between the SSH from late spring to early summer over the CETP and the SEP in CA, and the bimonthly correlation in April–May (AM, -0.51 , $P < 0.01$) is better than that in May–June (MJ, -0.44 , $P < 0.01$) and June–July (JJ, -0.34 , $P < 0.05$), which is comparable to the relationship in April–July (AMJJ, -0.53 , $P < 0.01$). This is mainly because the SSH over the TP in May is the strongest and its absolute variability is the highest in a through year (Yang et al. 2009; Zhao et al. 2018; Chen et al. 2019). The TP monsoon begins to onset in early June (Tang and Reiter 1984), and then the precipitation on the plateau begins to increase, leading to a significant decrease in SSH flux in June–July. Therefore, the relationship between the plateau SSH transport and the SEP in CA declines at this time.

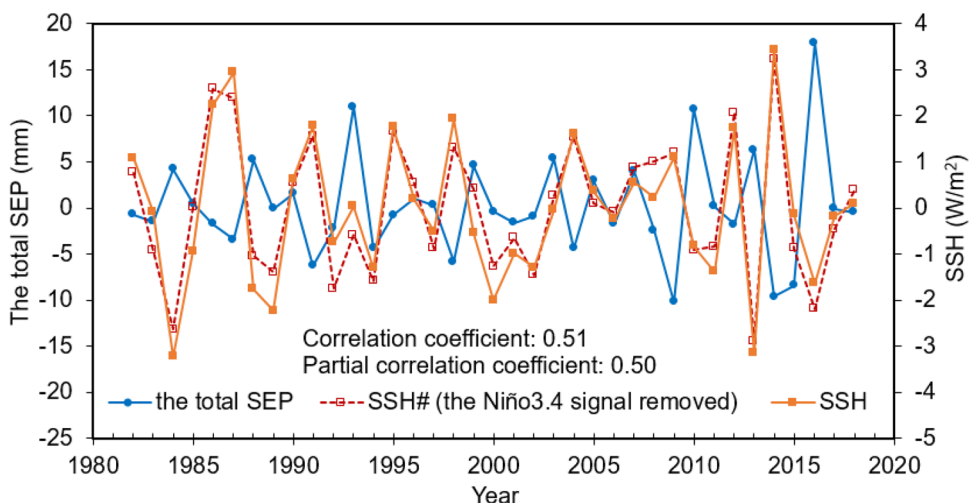
As ENSO is a dominant signal of the climate system in terms of the interannual variability, it is an important factor in regulating the interannual variation of precipitation in EA and South Asia in spring and summer (Mao and Wu 2007; Deng et al. 2016; Yu et al. 2021). Considering that the ENSO anomaly might influence the SEP in CA, we investigate the correlation coefficients between the Niño3.4 in different periods from April to July and the SEP in CA (Table 1). The correlation coefficient between the Niño3.4 in AM and the SEP in CA is only -0.11 , indicating that the AM Niño3.4 might not be correlated with the SEP in CA. But the bimonthly correlation improves significantly in MJ (-0.33 , $P < 0.05$) and JJ (-0.42 , $P < 0.01$), which indicates that there is also a significant negative correlation between ENSO and the SEP in CA in MJ and JJ, and the relationship in JJ even exceeds that between the SSH over the CETP and the SEP in CA. In order to explore the leading factor affecting the SEP in CA, we calculate the partial correlation coefficients between the SSH over the CETP and the SEP in CA with the Niño3.4 signal removed, and the partial correlation coefficients between the Niño3.4 and the SEP in CA with the SSH over the CETP signal removed in different periods from April to July (Table 1). It shows that their partial correlation coefficients decrease to a certain extent compared with the original correlation coefficients. Especially, the partial correlation coefficients between the AM, MJ and AMJJ Niño3.4 and the SEP in CA with the SSH signal removed decrease significantly, and the values become very small. That is to say, the partial correlation between the ENSO and the SEP in CA becomes very poor after removing the effect of the SSH over the CETP on the SEP in CA. By contrast, the partial correlations between the AM, MJ and AMJJ SSHs over the CETP and the SEP in CA with the Niño3.4 signal removed still present significant negative correlations ($P < 0.05$). Especially, the partial correlation coefficient between the AM SSH over the CETP and the SEP in CA after removing the Niño3.4 signal is -0.50 ($P < 0.01$), nearly the same as their original correlation (-0.51). From the interannual variation of the SSH over the CETP in AM (Fig. 4), it can be

Table 1 The correlation coefficients and partial correlation coefficients between the SEP in CA and the regional average SSH over the CETP and the Niño3.4 in different periods from April to July (# represents partial correlation coefficient)

Period	The correlation coefficients		Partial correlation coefficients	
	SSH	Niño3.4	SSH#	Niño3.4#
April–May	-0.51^{**}	-0.11	-0.50^{**}	0.07
May–June	-0.44^{**}	-0.33^*	-0.34^*	-0.16
June–July	-0.34^*	-0.42^{**}	-0.23	-0.35^*
April–July	-0.53^{**}	-0.30	-0.45^{**}	-0.04

*, **Statistical significance above the 95 and 99% confidence levels, respectively

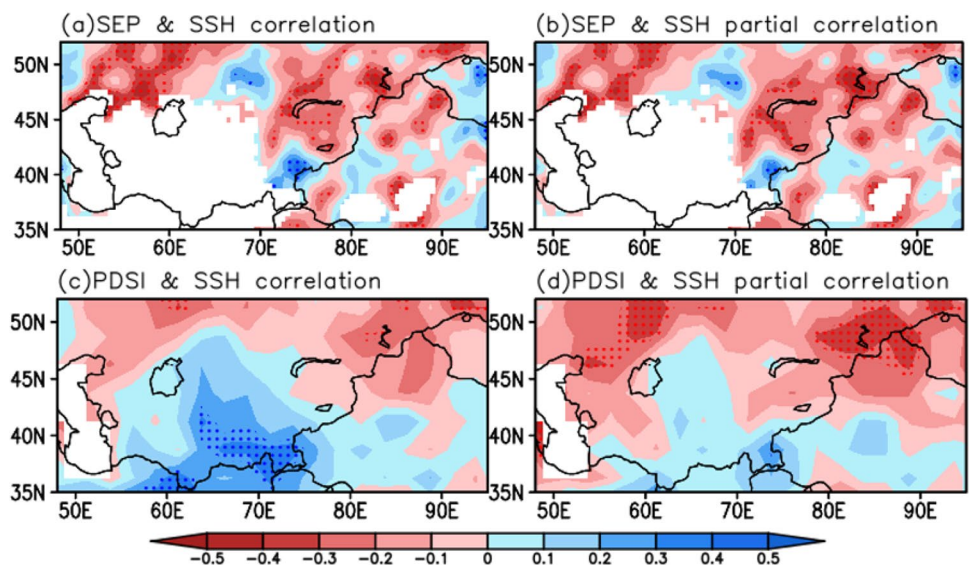
Fig. 4 The interannual variations of the regional average SSH and SSH# (the Niño3.4 signal removed) in AM over the CETP and the total SEP in CA during 1982–2018. The correlation coefficient and the partial correlation coefficient with the Niño3.4 signal removed between the SEP in CA and the AM SSH over the CETP are 0.51 and 0.50, respectively



seen that the SSH evolution with the Niño3.4 signal removed is very consistent with the original SSH, and the correlation coefficient reaches 0.94 ($P < 0.001$). Moreover, there is a good inverse relationship between the SSH over the CETP and the SEP in CA. That is, the anomalously strong AM SSH over the CETP corresponds to less SEP in CA, especially in 1986, 1987, 1991, 1998, 2004 and 2014. Otherwise, it corresponds to more extreme precipitation, especially in 1984, 1988, 2002, 2013 and 2016. It's worth noting that the partial correlation coefficient between the JJ Niño3.4 and the SEP in CA is -0.35 ($P < 0.05$), which is better than that between the JJ SSH over the CETP and the SEP in CA with the Niño3.4 signal removed. It indicates that the correlation between ENSO and the SEP in CA has been enhanced with the decrease of SSH transport over the CETP in early summer.

Then, what is the spatial distribution of the relationship between the SSH over the CETP and the SEP in CA? Where are the key areas? Does the SSH over the CETP also influence the summer drought in CA? To this end, the relationship between the summer PDSI and the AM SSH over the CETP is explored. Figure 5 shows the spatial distributions of correlation coefficients and partial correlation coefficients with the Niño3.4 signal removed between the SEP and the summer PDSI in CA and the AM SSH over the CETP. As can be seen, there is a significant negative correlation between the SSH over the CETP and the SEP in most parts of CA (Fig. 5a), which is consistent with the results in Table 1. The key areas with negative correlations are mainly in northeastern and northwestern CA and northern Xinjiang in China. Nevertheless, there are also some small areas with significant positive correlations, including Tajikistan,

Fig. 5 The spatial distributions of **a, c** the correlation coefficients and **b, d** the partial correlation coefficients with the Niño3.4 signal removed between **a, b** the SEP and **c, d** the summer PDSI in CA and the AM SSH over the CETP. The stippled areas in **a–d** indicate correlations above the 90% confidence level



Kyrgyzstan and central-northern part of Kazakhstan. As the extreme precipitation in southern CA is very rare, these grids with less than 20 samples of extreme precipitation data are removed in the correlation analysis between the SEP in CA and the SSH over the CETP. So, there are large blank areas in southern CA in Fig. 5a, b. The spatial distribution of the correlation coefficients between the summer PDSI in CA and the AM SSH over the CETP shows a south–north dipole mode, with significant positive correlations in southern CA and negative correlations in northern CA and northern Xinjiang in China (Fig. 5c). It resembles the correlation map between the SEP in CA and the AM SSH over the CETP, indicating that the strong SSH over the CETP in late spring facilitates less SEP in northern CA and the summer drought will intensify (alleviate) in northern (southern) CA, and vice versa. The spatial patterns of the partial correlation coefficients with the Niño3.4 signal removed (Fig. 5b, d) are similar to the original correlation patterns (Fig. 5a, c). The partial correlation coefficient is more significant than the original correlation coefficient between the summer PDSI and the SSH over the CETP in northern CA and northern

Xinjiang. Therefore, we can conclude that in late spring (before the TP monsoon onset), the SSH over the CETP can affect the SEP and the summer drought in CA, which is independent of ENSO.

5 Key circulation systems

The above analysis shows that there are good correlations between the AM SSH over the CETP and both the SEP and the summer drought in CA. Then, how is the connection established? Regression analyses between the AM SSH over the CETP and the bimonthly geopotential height fields at 500-hPa, 300-hPa and 100-hPa from April to August are conducted (Fig. 6). According to the thermal adaptation theory (Wu et al. 2007, 2016; Liu et al. 2017b), the anomalously enhanced thermal effect of the plateau surface will cause the lower atmosphere to be heated, converge and rise, forming a thermal low pressure at the low levels over the TP. Accordingly, the geopotential height will increase anomalously in the upper levels, forming a warm high pressure

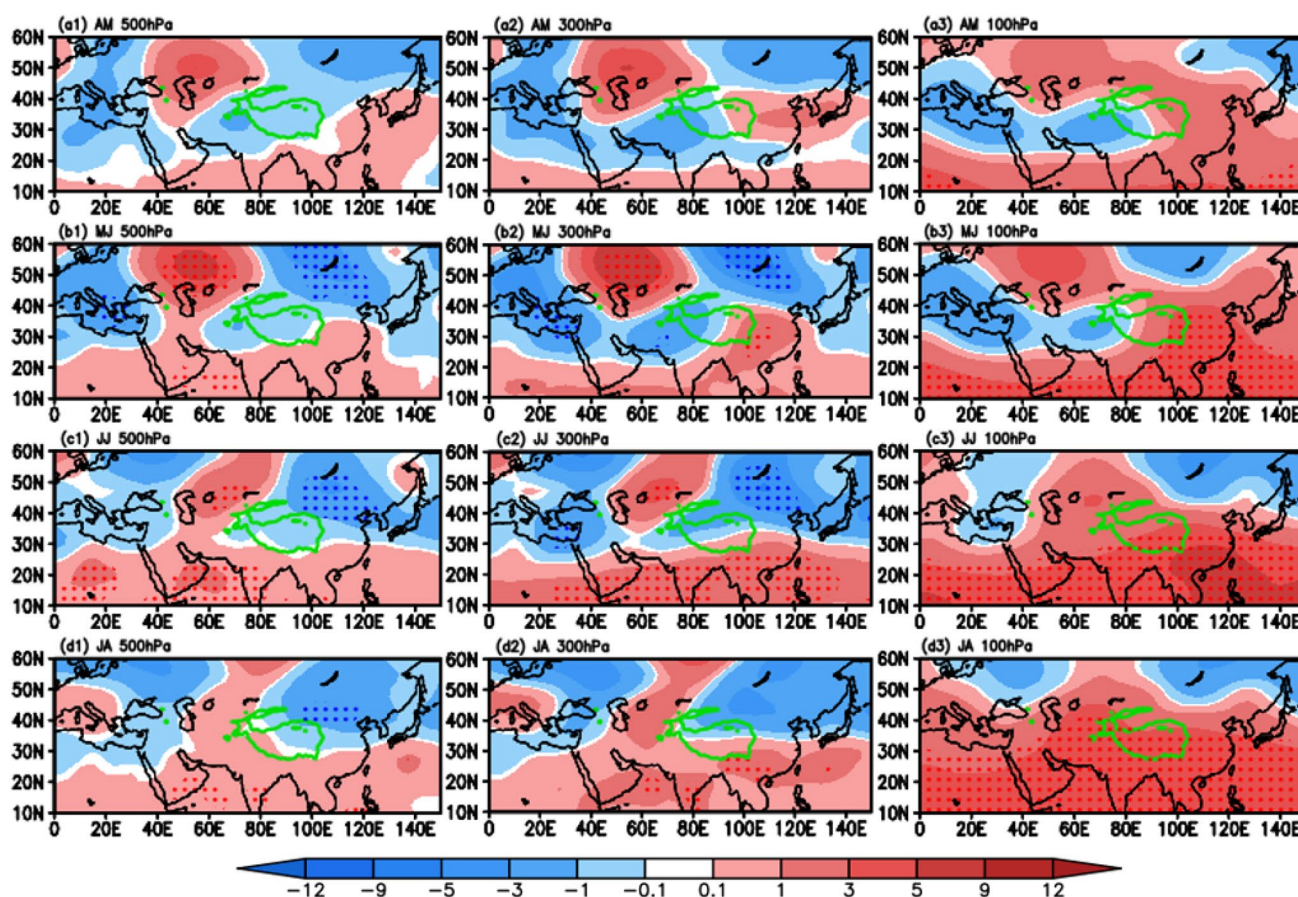


Fig. 6 Regression fields between the average AM SSH over the CETP and the bimonthly geopotential height (units: dagpm) at 500-hPa, 300-hPa and 100-hPa in **a** AM, **b** MJ, **c** JJ and **d** JA. The green

solid curves in **a–d** denote the TP domain with altitude higher than 3000 m a.s.l., and the stippled areas in **a–d** indicate correlations above the 95% confidence level

center there. In Fig. 6, with the anomalous enhancement of sensible heat on the CETP in AM, the 500-hPa geopotential height is anomalously low in AM (Fig. 6a1), the 300-hPa geopotential height over the eastern TP is anomalously high (Fig. 6a2), and the 100-hPa geopotential height anomaly is further enhanced (Fig. 6a3). In MJ, the geopotential height anomaly at 300-hPa over the eastern plateau and the low-latitude areas is further intensified (Fig. 6b2), and it is significantly enhanced at 100-hPa (Fig. 6b3). In the following JJ and JA, the anomalous intensification of 100-hPa geopotential height develops further, with significant anomaly dominating in the south of 40° N. Previous studies indicated that the SSH transportation over the TP from spring to summer has a good persistence (Wang and Li 2019). When the SSH is anomalously intense in spring, the SSH transportation in the following summer will be anomalously strong. Thus, the anomalously strong SSH on the TP in AM will be transmitted from the lower to the upper layers through the continuous heating to the atmosphere. It will eventually be preserved in the upper troposphere for a long time, resulting in an anomalously strong South Asia High (SAH) afterwards, and vice versa. The SAH, also known as the Tibetan high (Ye and Gao 1979), is the strongest and most stable circulation system at 100-hPa in the Northern Hemisphere in summer. Numerous studies have indicated that the formation and development of the SAH are closely related to the thermal effect of the TP. Both diagnostic analysis and numerical simulation have confirmed that the sensible and latent heating of the TP play an essential role in the formation and evolution of the SAH (Wu et al. 1999; Liu et al. 2004; Ren et al. 2019; Zhang et al. 2019b). To verify whether the SSH anomalies over the CETP regulate the SEP in CA by influencing the SAH, the composite analysis is carried out for the atmospheric circulations in the Northern Hemisphere in summer. We investigate the differences between strong and weak SSH years, providing an insight into the physical processes and the key circulation systems in which the plateau sensible heat influences the SEP and the summer drought in CA. According to the time series of AM SSH over the CETP with Niño3.4 signal removed, and taking one standard deviation as the abnormal standard, six strong SSH years (1986, 1987, 1991, 1995, 2012 and 2014) and six weak SSH years (1984, 1992, 1994, 2002, 2013 and 2016) are selected. As 1987, 1991, 1992 and 2016 are strong El Niño years, considering the possible influences of ENSO on atmospheric circulations, the cases in these four years are removed. Finally, four strong SSH years (1986, 1995, 2012 and 2014) and four weak SSH years (1984, 1994, 2002 and 2013) are selected to conduct the composite analysis.

Figure 7 shows the distribution of summer average geopotential height at 100-hPa during 1982–2018 and the composite geopotential height anomaly at 100-hPa in strong and weak SSH years in AM. As can be seen, the summer average SAH is located over the TP and the Iranian plateau (Fig. 7a).

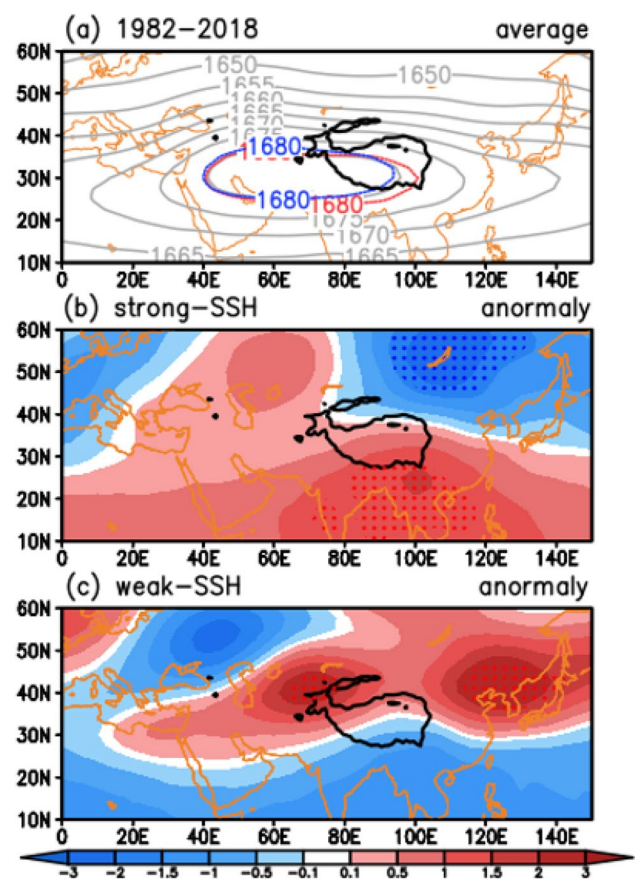


Fig. 7 a Distributions of summer average geopotential height (units: dagpm) at 100-hPa during 1982–2018, and the composite geopotential height anomalies at 100-hPa in the **b** strong SSH years and **c** weak SSH years in AM over the CETP. The red (blue) dashed line in **a** denote the location of SAH in the strong (weak) years. The black heavy solid curves in **a–c** denote the TP, and the stippled areas in **b** and **c** indicate the anomalies above the 90% confidence level

When the SSH over the CETP is anomalously strong in late spring (AM), the 100-hPa geopotential height in summer is significantly increased over the TP and the lower latitudes south of it (Fig. 7b), and the SAH is anomalously strong and eastward (Fig. 7a). Conversely, when the SSH is anomalously weak over the CETP, the geopotential height is anomalously low over the southern plateau and the low latitudes, an anomalously high appears over the CA, northern China and Japanese archipelago (Fig. 7c), and the SAH is anomalously weak and westward (Fig. 7a). The results are consistent with those in Fig. 6, that is, the strong SSH anomaly will result in an anomalously strong SAH, and vice versa.

Figure 8 illustrates the distribution of summer subtropical westerly jet at 200-hPa during 1982–2018, and the average and composite zonal wind anomalies at 200-hPa in the strong and weak SSH years in AM over the CETP. As shown in Fig. 8a, the average subtropical westerly jet in summer is located in 36° N–45° N, with the jet center ($U > 25$ m/s) in

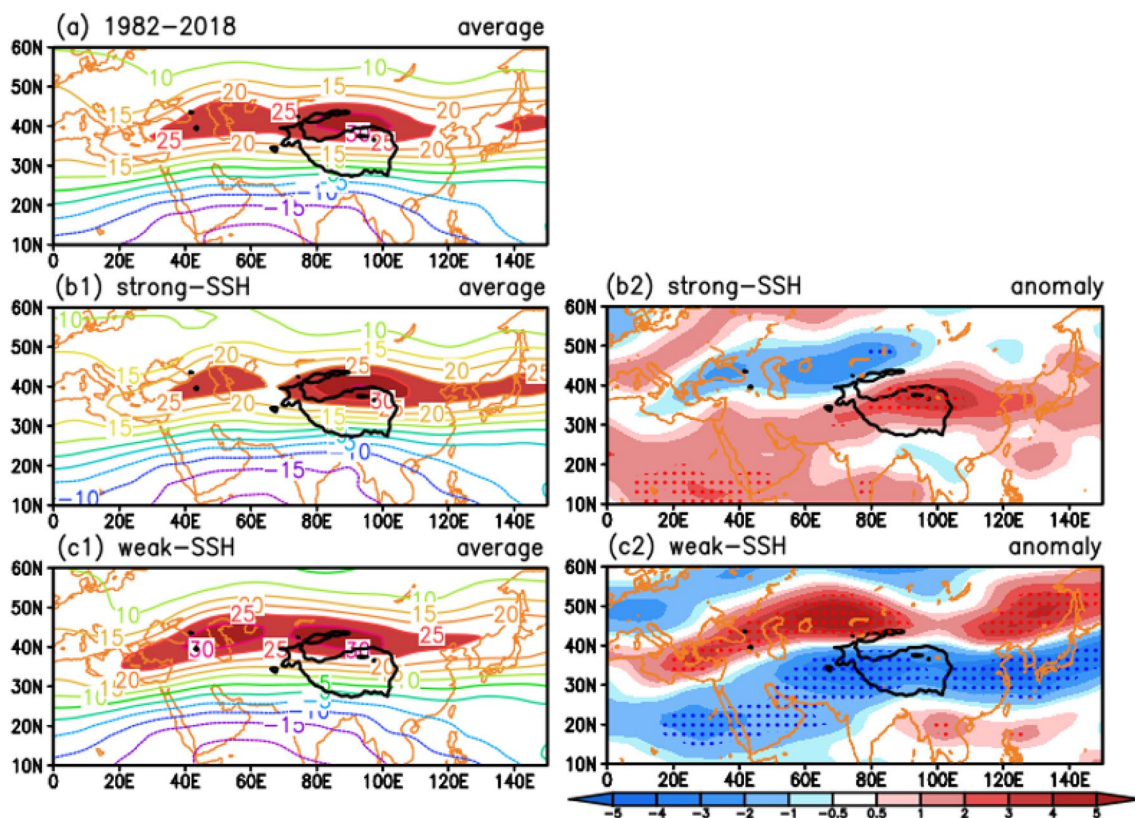


Fig. 8 a Distributions of summer average zonal wind (units: m s^{-1}) at 200-hPa during 1982–2018, and **b1**, **c1** the average and **b2**, **c2** the composite zonal wind anomalies at 200-hPa in the **b1**, **b2** strong and

c1, **c2** weak SSH years in AM over the CETP. The black heavy solid curves in **a–c** denote the TP, and the stippled areas in **b** and **c** indicate the anomalies above the 90% confidence level

the north of the TP. When the SSH over the CETP in late spring (AM) is anomalously strong, the westerly anomalies over the TP and its east strengthen, and the easterly anomalies appear over CA (Fig. 8b2). So the subtropical westerly jet is anomalously weak over CA and anomalously strong over the north part of TP, and the location of the westerly jet is slightly southward (Fig. 8b1), compared with the climate mean (Fig. 8a). When the plateau SSH is anomalously weak in late spring (AM), there is an opposite situation. In 15°N – 35°N , the easterly anomalies significantly strengthen over West Africa, the Arabian Peninsula, the Iranian plateau, the TP and its east, and the Japanese archipelago. In 35°N – 50°N , the westerly anomalies intensify over the Mediterranean, the south of Ural Mountains, northern CA and northern China (Fig. 8c2). Thus, the subtropical westerly jet is anomalously strong and northward with the northern boundary of the jet center ($U > 25 \text{ m/s}$) near 48°N (Fig. 8c1). The variations of the subtropical westerly jet from April to July in strong and weak years are also investigated (figures not shown), and the results are similar to those in summer. That is, the strong (weak) SSH anomaly over the CETP facilitates the subtropical westerly jet to be anomalously weak (strong) and southward (northward) over CA.

The 500-hPa geopotential height and temperature fields (Fig. 9) show that, when the SSH over the CETP in late spring (AM) is anomalously strong (Fig. 9b1), the geopotential height is anomalously high over the south of 30°N and northern CA in summer. The subtropical high over northern Africa, the Arabian Peninsula and the western Pacific is anomalously strong, the Ural ridge strengthens and CA trough weakens (Fig. 9a, b1). The northern CA is controlled by an abnormal warm high-pressure ridge (Fig. 9b1, b2), which is not conducive to the generation of extreme precipitation in the region. Conversely, when the SSH over the CETP in late spring (AM) is anomalously weak (Fig. 9c1), the geopotential height is anomalously low over the south of 30°N and northern CA in summer. The subtropical high over northern Africa, the Arabian Peninsula and the western Pacific is anomalously weak, the Ural ridge weakens and the CA trough strengthens (Fig. 9a, c1). The northern CA and northern Xinjiang in China are controlled by an abnormal cold low-pressure trough (Fig. 9c1, c2), which is conducive to the generation of extreme precipitation in these regions. Moreover, the western TP and its vicinity are controlled by an abnormal warm high-pressure ridge, which is not conducive to the generation of extreme precipitation in Tajikistan and Kyrgyzstan of southeastern CA.

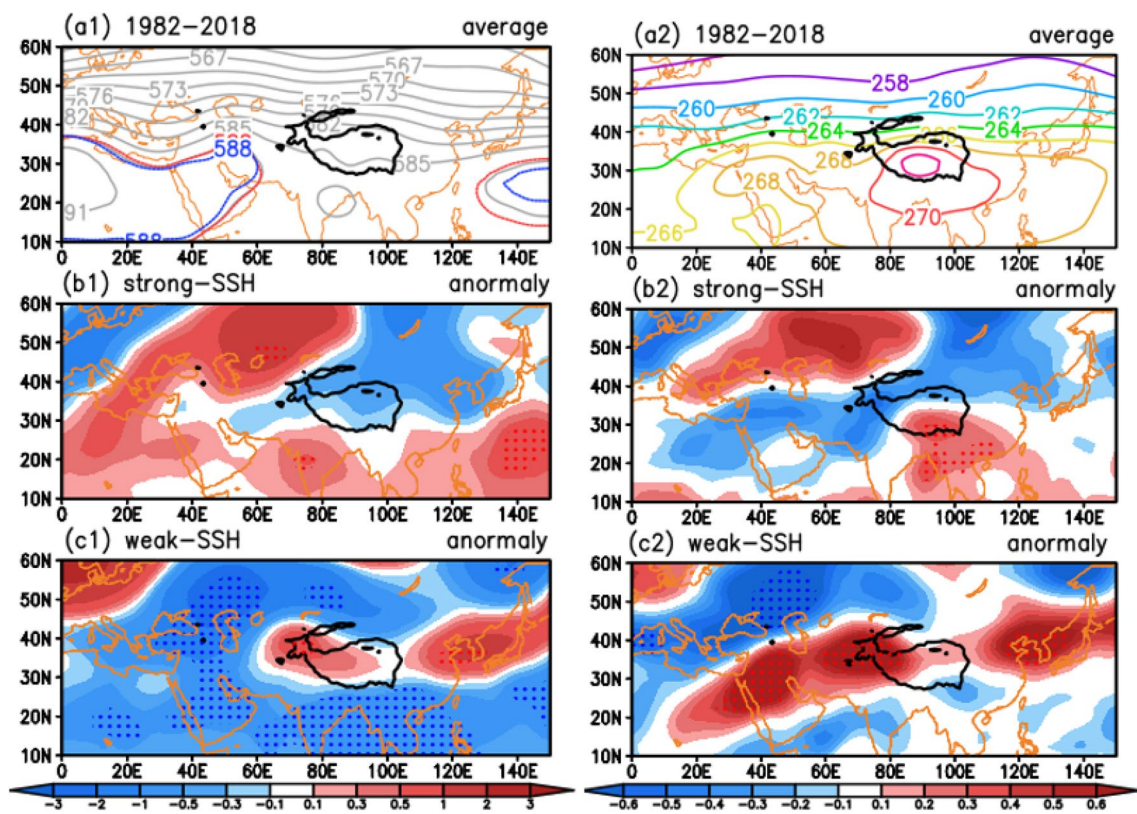


Fig. 9 The same as Fig. 7, but for 500-hPa (a1–c1) geopotential height (units: dagpm) and (a2–c2) temperature (units: K)

The 850-hPa wind field (Fig. 10) also indicates that when the SSH over the CETP is anomalously strong in late spring (AM), the anticyclonic circulation anomaly in northern CA is strengthened in summer (Fig. 10a, b). Figure 11 shows the distributions of moisture flux and moisture flux divergence at different levels and for the whole layer in summer over the CETP in strong and weak SSH years. The anomalous water vapor from the Mediterranean and the North Atlantic flows into CA from its northern and eastern boundaries via the Barents Sea and the West Siberian plain, forming significant divergence in northern CA (Fig. 11a1–d1). It is not conducive the generation of extreme precipitation, and intensifies the summer drought in the region. Conversely, when the plateau SSH is anomalously weak (Fig. 10c), the CA and its adjacent regions are controlled by an abnormal cyclonic circulation, which weakens the Ural ridge and strengthens the CA trough, facilitating water vapor to enter CA through its western and southern boundaries. The distribution of moisture flux at 925-hPa indicates that the anomalous water vapor from the Arctic Ocean and the North Atlantic converges in southwestern CA through its western boundary (Fig. 11a2). Due to the terrain blocking effect of the TP and Pamirs and Iranian plateaus, there is little water vapor entering CA through the southern boundary in the lower troposphere. However, at the middle troposphere (700-hPa

and 500-hPa), the anomalous water vapor from the Western Pacific, the South China Sea and the Bay of Bengal entering CA through the southern boundary increases rapidly, and is transported northward along the southwest airflow in front of the CA trough, then forming the convergence in northern CA (Fig. 11b2, c2). The distribution of the whole layer moisture flux also shows that there are three water vapor sources entering CA, namely two sources from the Arctic and North Atlantic entering CA through the western boundary, and one source from the western Pacific, the South China Sea and the Bay of Bengal entering CA through the southern boundary. These anomalous water vapor converges in northern CA and northern Xinjiang (Fig. 11d2), which is conducive to the generation of widespread extreme precipitation and the alleviation of summer drought in these regions.

To sum up, The SSH anomalies over the CETP can affect the SEP and summer drought in CA by regulating the location and strength of the SAH and the subtropical jet. The strong SSH anomalies over the CETP in late spring (AM) can lead to the anomalously strong and eastward SAH in summer, anomalously weak subtropical westerly jet over CA and anomalously strong subtropical high over north Africa, the Arabian Peninsula and the western Pacific. In addition, the Ural ridge strengthens, the CA trough weakens, and the northern CA is controlled by an abnormal warm high-pressure ridge with less water vapor

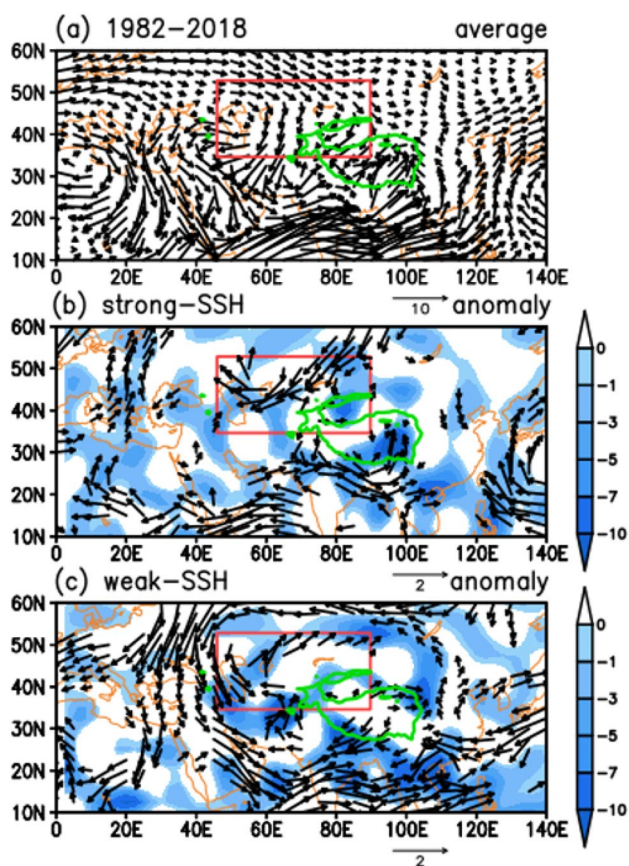


Fig. 10 The same as Fig. 7, but for 850-hPa wind (units: m s^{-1} , vectors) and the divergence (shading, 10^{-7} s^{-1}). The black vectors in **b**, **c** denote the anomalies above the 90% confidence level

convergence. All these circulation characteristics are not conducive to the generation of extreme precipitation in northern CA, so the summer drought will intensify. Conversely, the weak SSH anomalies over the CETP in late spring (April–May) can result in the anomalously weak SAH in summer, anomalously strong and northward subtropical westerly jet, and the anomalously weak subtropical high in north Africa, the Arabian Peninsula and the western Pacific. In addition, CA and its adjacent regions are controlled by abnormal cyclonic circulation, which weakens the Ural ridge and strengthens the CA trough. At the same time, the anomalous water vapor from the Arctic, North Atlantic, the western Pacific, the south China sea and the Bay of Bengal, converges in northern CA and northern Xinjiang, which is conducive to the generation of widespread extreme precipitation and the alleviation of summer drought in these regions.

6 Conclusions and discussion

In this study, the SEP threshold, total amount of SEP and the number of SEP days in CA are calculated by the international percentile method. Furthermore, the relationships

between SEP and summer drought in CA and the SSH transport over the CETP from late spring to early summer are discussed. The main conclusions are as follows.

The distribution of SEP in CA is extremely uneven, and the extreme precipitation thresholds range from 2 to 32 mm/day, with large regional differences. Both the total amount of SEP and the number of SEP days show significant increasing trends, with the climatic tendencies of 4.4 mm/decade and 0.4 day/decade, respectively. Extreme weather events in CA are intensifying. The SSH over the CETP in late spring (April–May) is well related to the SEP and summer drought in CA. Significant negative correlations are found in northwestern-northeastern CA and northern Xinjiang of China. That is, the anomalously strong (weak) SSH in late spring over the CETP will lead to anomalously less (more) SEP in northern CA and northern Xinjiang, and the summer drought will be intensified (alleviated).

The SSH anomalies over the CETP can affect the SEP and summer drought in CA by regulating the location and strength of the SAH and the subtropical jet over CA. When the SSH over the CETP is anomalously weak in late spring (AM), the key circulation factors leading to frequent SEP in northern CA are as follows: the anomalously weak SAH, the subtropical westerly jet strengthened over the CA and weakened over the TP and EA, the anomalously weak north Africa subtropical high, and the strengthened CA trough. In addition, there are three water vapor sources, namely the sources from the Arctic and North Atlantic entering CA through the western boundary, and the source from the western Pacific, the South China Sea and the Bay of Bengal entering CA through the southern boundary. They provide sufficient water vapor for the extreme precipitation in northern CA.

This study provides an insight into the influence of the TP thermal effect on the extreme precipitation and summer drought in CA. Previous studies have shown that the anomalously strong (weak) SSH over the TP in spring can lead to anomalously less (more) summer precipitation in southern China (the Yangtze River valley) (Hsu and Liu 2003; Cui et al. 2015). This study also shows that the circulation systems over EA are significantly different in the years with anomalously strong and weak SSH over the CETP. The anomalously weak SSH over the CETP in late spring can result in the anomalously weak subtropical high over the western Pacific in summer (Fig. 9a1, 9c1). The southern China is controlled by an abnormal cyclonic circulation (Fig. 10c) and water vapor convergence (Fig. 11a2–d2), while the Yangtze River valley and the Japanese Islands are controlled by an anticyclonic circulation (Fig. 10c) and water vapor divergence (Fig. 11a2–d2). Such situations are conducive to the generation of summer precipitation in southern China, but not conducive to the summer precipitation in the Yangtze River valley and the Japanese Islands.

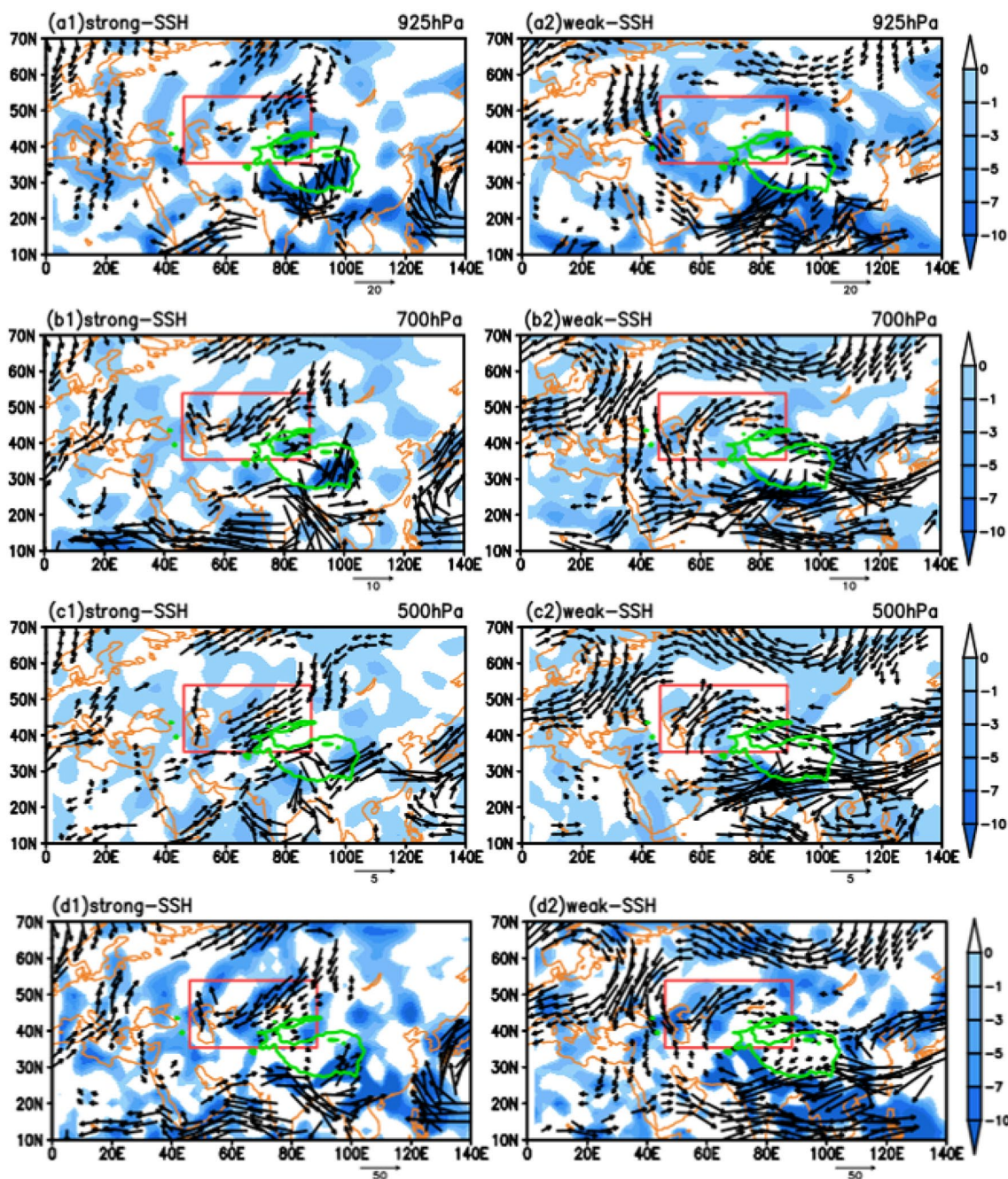


Fig. 11 The distributions of moisture flux (vector; units: $\text{kg m}^{-1} \text{s}^{-1}$) and moisture flux divergence (shading; units: $10^{-6} \text{ kg m}^{-2} \text{ s}^{-1}$) in summer over the CETP for **a** 925-hPa, **b** 700-hPa and **c** 500-hPa and

d the whole layer (from ground to 300-hPa). Figures **a1–d1** are for strong SSH years, and figures **a2–d2** are for weak SSH years. The black vectors denote the anomalies above the 90% confidence level

These results indicate that the SSH anomaly over the CETP can affect the climate of CA and EA simultaneously, and the SSH variation in late spring over the CETP can be an effective predictor for the climate of CA and EA.

However, due to the complex topography of the TP, the SSH variations are inconsistent over different areas (Duan et al. 2011; Wang et al. 2019). Thus, the key areas for the influence of the plateau SSH anomalies on the SEP and summer drought

in CA, and the effective simplification of forecast indicators will be further investigated. In addition, some questions remain to be addressed. For example, whether the SEP and summer drought in CA are mainly influenced by the surface thermal effect over the CETP, and whether the relationship is regulated by other external forcing factors, such as NAO. The NAO has been proven to be an important influence factor for the precipitation anomaly in CA, and it also has a significant impact on

the climate of the TP. Cui et al. (2015) pointed out that during the positive phase of NAO in winter, it can excite a stable downstream Rossby wave train, inducing the Asian subtropical westerly jet to intensify and the India–Burma trough to deepen, and it can also increase the snow depth over the TP in winter. Other research has reported that the March surface air temperature over the TP is closely related to the February NAO and regulated by the phase of the Atlantic multi-decadal variability (Li et al. 2021). Therefore, the SEP in CA is directly influenced by the spring SSH over the TP, and may also be modulated by the winter SST anomalies in the North Atlantic. What are the synergetic effect and contribution rates of the NAO and the SSH over the CETP? These issues deserve further study.

Acknowledgements This work was supported by the Key Project of National Key Research and Development Program of China (2018YFC1507101), and the Second Tibetan Plateau Scientific Expedition and Research (STEP) program (2019QZKK0103). We are grateful to four anonymous reviewers for the thorough reviews and critical comments. We also thank Nanjing Hurricane Translation for reviewing the English language quality of this paper.

Author contributions JZ, DL and HW contributed to the study conception and design. Material preparation and data collection were performed by LC and HW. Analysis was performed by HW, DL, JZ, and LC. The first draft of the manuscript was written by HW and all authors commented on previous versions of the manuscript. All authors read and approved the final manuscript.

Declarations

Conflict of interest The authors declare that they have no conflict of interest.

Open Access This article is licensed under a Creative Commons Attribution 4.0 International License, which permits use, sharing, adaptation, distribution and reproduction in any medium or format, as long as you give appropriate credit to the original author(s) and the source, provide a link to the Creative Commons licence, and indicate if changes were made. The images or other third party material in this article are included in the article's Creative Commons licence, unless indicated otherwise in a credit line to the material. If material is not included in the article's Creative Commons licence and your intended use is not permitted by statutory regulation or exceeds the permitted use, you will need to obtain permission directly from the copyright holder. To view a copy of this licence, visit <http://creativecommons.org/licenses/by/4.0/>.

References

- Aizen EM, Aizen VB, Melack JM et al (2001) Precipitation and atmospheric circulation patterns at mid-latitudes of Asia. *Int J Climatol* 21:535–556. <https://doi.org/10.1002/joc.626>
- Alexander LV (2016) Global observed long-term changes in temperature and precipitation extremes: a review of progress and limitations in IPCC assessments and beyond. *Weather Clim Extr* 11:4–16. <https://doi.org/10.1016/j.wace.2015.10.007>
- Bonsal BR, Zhang X, Vincent LA et al (2001) Characteristics of daily and extreme temperatures over Canada. *J Clim* 14:1959–1976. [https://doi.org/10.1175/15200442\(2001\)014%3c1959:CODAET%3e2.0.CO;2](https://doi.org/10.1175/15200442(2001)014%3c1959:CODAET%3e2.0.CO;2)
- Bothe O, Fraedrich K, Zhu XH (2012) Precipitation climate of Central Asia and the large-scale atmospheric circulation. *Theor Appl Climatol* 108:345–354. <https://doi.org/10.1007/s00704-011-0537-2>
- Chen LX, Reiter ER, Feng ZQ (1985) The atmospheric heat source over the Tibetan Plateau: May–August 1979. *Mon Weather Rev* 113(10):1771–1790. [https://doi.org/10.1175/1520-0493\(1985\)113%3c1771:TAHSOT%3e2.0.CO;2](https://doi.org/10.1175/1520-0493(1985)113%3c1771:TAHSOT%3e2.0.CO;2)
- Chen MY, Shi W, Xie PP et al (2008) Assessing objective techniques for gauge based analyses of global daily precipitation. *J Geophys Res Atmos* 113:D04110. <https://doi.org/10.1029/2007JD009132>
- Chen FH, Wang JS, Jin LY et al (2009) Rapid warming in mid-latitude central Asia for the past 100 years. *Front Earth Sci China* 3:42–50. <https://doi.org/10.1007/s11707-009-0013-9>
- Chen FH, Huang W, Jin LY et al (2011) Spatiotemporal precipitation variations in the arid Central Asia in the context of global warming. *Sci China Earth Sci* 54:1812–1821. <https://doi.org/10.1007/s11430-011-4333-8>
- Chen YN, Li Z, Li WH et al (2016) Water and ecological security: dealing with hydroclimatic challenges at the heart of China's Silk Road. *Environ Earth Sci* 75:881. <https://doi.org/10.1007/s12665-016-5385-z>
- Chen L, Pryor SC, Wang H et al (2019) Distribution and variation of the surface sensible heat flux over the central and eastern Tibetan Plateau: comparison of station observations and reanalysis products. *J Geophys Res Atmos* 124:6191–6206. <https://doi.org/10.1029/2018JD030069>
- Cui YF, Duan AM, Liu YM et al (2015) Interannual variability of the spring atmospheric heat source over the Tibetan Plateau forced by the North Atlantic SSTA. *Clim Dyn* 45:1617–1634. <https://doi.org/10.1007/s00382-014-2417-9>
- Dai AG, Trenberth KE, Qian TT (2004) A global dataset of palmer drought severity index for 1870–2002: relationship with soil moisture and effects of surface warming. *J Hydrometeorol* 5(6):1117–1130. https://journals.ametsoc.org/view/journals/hydr/5/6/-jhm386_1.xml
- Deng MY, Lu RY, Chen W et al (2016) Interannual variability of precipitation in May over the South Asian monsoonal region. *Int J Climatol* 36(4):1724–1732. <https://doi.org/10.1002-joc.4454>
- Donat MG, Lowry AL, Alexander LV et al (2016) More extreme precipitation in the world's dry and wet regions. *Nat Clim Change* 6:508–513. <https://doi.org/10.1038/NCLIMATE2941>
- Duan AM, Wu GX (2005) Role of the Tibetan Plateau thermal forcing in the summer climate patterns over subtropical Asia. *Clim Dyn* 24:793–880. <https://doi.org/10.1007/s00382-004-0488-8>
- Duan AM, Li F, Wang MR et al (2011) Persistent weakening trend in the spring sensible heat source over the Tibetan Plateau and its impact on the Asian summer monsoon. *J Clim* 24(21):5671–5682. <https://doi.org/10.1175/JCLI-D-11-00052.1>
- Duan AM, Sun RZ, He JH (2017) Impact of surface sensible heating over the Tibetan Plateau on the western Pacific subtropical high: a land-air-sea interaction perspective. *Adv Atmos Sci* 34(2):157–168. <https://doi.org/10.1007/s00376-016-6008-zg>
- Duchon CE (1979) Lanczos filtering in one and two dimensions. *J Appl Meteorol Clim* 18(8):1016–1022. [https://doi.org/10.1175/15200450\(1979\)018%3c1016:LFOAT%3e2.0.CO;2](https://doi.org/10.1175/15200450(1979)018%3c1016:LFOAT%3e2.0.CO;2)
- Filippi L, Palazzi E, von Hardenberg J et al (2014) Multidecadal variations in the relationship between the NAO and winter precipitation in the HinduKush–Karakoram. *J Clim* 27:7890–7902. <https://doi.org/10.1175/JCLI-D-14-00286.1>
- Hsu HH, Liu X (2003) Relationship between the Tibetan plateau heating and east Asian summer monsoon rainfall. *Geophys Res Lett* 30(20):2066. <https://doi.org/10.1029/2003gl017909>

- Hu ZY, Zhang C, Hu Q et al (2014) Temperature changes in central Asia from 1979 to 2011 based on multiple datasets. *J Clim* 27:1143–1167. <https://doi.org/10.1175/JCLI-D-13-00064.1>
- Hu ZY, Li QX, Chen X et al (2016) Climate changes in temperature and precipitation extremes in an alpine grassland of Central Asia. *Theor Appl Climatol* 126:519–531. <https://doi.org/10.1007/s00704-015-1568-x>
- Huang JP, Chen W, Wen ZP et al (2019) Review of Chinese atmospheric science research over the past 70 years: climate and climate change. *Sci China Earth Sci* 62:1514–1550. <https://doi.org/10.1007/s11430-019-9483-5>
- IPCC (2014) Climate Change 2014: impacts, adaptation and vulnerability. In: Contribution of Working Group II to the fifth assessment report of the Intergovernmental Panel on Climate Change. Cambridge University Press, Cambridge, p 151
- Li J, Wang B (2017) Predictability of summer extreme precipitation days over eastern China. *Clim Dyn* 51:4543–4554. <https://doi.org/10.1007/s00382-017-3848-x>
- Li CF, Zhang C, Luo GP et al (2015) Carbon stock and its responses to climate change in Central Asia. *Glob Change Biol* 21:1951–1967. <https://doi.org/10.1111/gcb.12846>
- Li PY, Qian H, Zhou W (2017) Finding harmony between the environment and humanity: an introduction to the thematic issue of the Silk Road. *Environ Earth Sci* 76:105. <https://doi.org/10.1007/s12665-017-6428-9>
- Li JY, Li F, He SP et al (2021) The Atlantic multidecadal variability phase dependence of teleconnection between the North Atlantic Oscillation in February and the Tibetan Plateau in March. *J Clim* 34(11):4227–4242. <https://journals.ametsoc.org/view/journals/clim/34/11/JCLI-D-20-0157.1>
- Liu YM, Wu GX, Ren RC (2004) Relationship between the subtropical anticyclone and diabatic heating. *J Clim* 17(4):682–698. [https://doi.org/10.1175/15200442\(2004\)017-%3c0682:RBT-SAA%3e2.0.CO;2](https://doi.org/10.1175/15200442(2004)017-%3c0682:RBT-SAA%3e2.0.CO;2)
- Liu Y, Wu GX, Hong J et al (2012) Revisiting Asian monsoon formation and change associated with Tibetan Plateau forcing: II. *Change Clim Dyn* 39:1183–1195. <https://doi.org/10.1007/s00382-012-1335-y>
- Liu H, Liu XD, Dong BW (2017a) Intraseasonal variability of winter precipitation over central Asia and the western Tibetan Plateau from 1979 to 2013 and its relationship with the North Atlantic Oscillation. *Dyn Atmos Oceans* 79:31–42. <https://doi.org/10.1016/j.dynatmoce.2017.07.001>
- Liu YM, Wang ZQ, Zhuo HF et al (2017b) Two types of summertime heating over Asian large-scale orography and excitation of potential-vorticity forcing II. Sensible heating over Tibetan-Iranian Plateau. *Sci China Earth Sci* 60:733–744. <https://doi.org/10.1007/s11430-016-9016-3>
- Liu YZ, Wu CQ, Jia R et al (2018) An overview of the influence of atmospheric circulation on the climate in arid and semi-arid region of Central and East Asia. *Sci China Earth Sci* 61:1183–1194. <https://doi.org/10.1007/s11430-017-9202-1>
- Liu X, Jia X, Wang M et al (2021) The impact of Tibetan Plateau snow cover on the summer temperature in Central Asia. *Adv Atmos Sci*. <https://doi.org/10.1007/s00376-021-1011-4>
- Lu MM, Yang S, Li ZN et al (2018) 2018: possible effect of the Tibetan Plateau on the “upstream” climate over West Asia, North Africa, South Europe and the North Atlantic. *Clim Dyn* 51:1485–1498. <https://doi.org/10.1007/s00382-017-3966-5>
- Ma WQ, Ma YM (2016) Modeling the influence of land surface flux on the regional climate of the Tibetan Plateau. *Theor Appl Climatol* 125(1):45–52. <https://doi.org/10.1007/s00704-015-1495-x>
- Mao JY, Wu GX (2007) Interannual variability in the onset of the summer monsoon over the Eastern Bay of Bengal. *Theor Appl Climatol* 89(3–4):155–170. <https://doi.org/10.1007/s00704-006-0265-1>
- Peng DD, Zhou TJ, Zhang LX et al (2019) Detecting human influence on the temperature changes in central Asia. *Clim Dyn* 53(7):4553–4568. <https://doi.org/10.1007/s00382-019-04804-2>
- Pryor SC, Howe JA, Kunkel KW (2009) How spatially coherent and statistically robust are temporal changes in extreme precipitation in the contiguous USA? *Int J Climatol* 29(1):31–45. <https://doi.org/10.1002/joc.1696>
- Rana S, McGregor J, Renwick J (2017) Wintertime precipitation climatology and ENSO sensitivity over central southwest Asia. *Int J Climatol* 37:1494–1509. <https://doi.org/10.1002/joc.4793>
- Ren ZH, Yu Y, Zou FL et al (2012) Quality detection of surface historical basic meteorological data. *J Appl Meteorol Sci* 23(6):739–747 ((in Chinese))
- Ren ZG, Zhang MJ, Wang SJ et al (2015) Changes in daily extreme precipitation events in South China from 1961 to 2011. *J Geogr Sci* 25:58–68. <https://doi.org/10.1007/s11442-015-1153-3>
- Ren RC, Zhu CD, Cai M (2019) Linking quasi-biweekly variability of the South Asian high to atmospheric heating over Tibetan Plateau in summer. *Clim Dyn* 53:3419–3429. <https://doi.org/10.1007/s00382-019-04713-4>
- Schiemann R, Lüthi D, Schä C (2009) Seasonality and interannual variability of the westerly jet in the Tibetan Plateau region. *J Clim* 22:2940–2957. <https://doi.org/10.1175/2008JCLI2625.1>
- Shang W, Li SS, Ren XJ et al (2020) Event-based extreme precipitation in Central-Eastern China: large-scale anomalies and teleconnections. *Clim Dyn* 54:2347–2360. <https://doi.org/10.1007/s00382-019-05116-1>
- Shi Y, Shen Y, Kang E et al (2007) Recent and future climate change in Northwest China. *Clim Change* 80:379–393. <https://doi.org/10.1007/s10584-006-9121-7>
- Skansi MM, Brunet M, Sigró J et al (2013) Warming and wetting signals emerging from analysis of changes in climate extreme indices over South America. *Glob Planet Change* 100:295–307. <https://doi.org/10.1016/j.gloplacha.2012.11.004>
- Sun H, Liu X (2021) Impacts of dynamic and thermal forcing by the Tibetan Plateau on the precipitation distribution in the Asian arid and monsoon regions. *Clim Dyn* 56:2339–2358. <https://doi.org/10.1007/s00382-020-05593-9>
- Sun RZ, Duan AM, Chen LL et al (2019a) Interannual variability of the north pacific mixed layer associated with the spring Tibetan Plateau thermal forcing. *J Clim* 32(11):3109–3130. <https://doi.org/10.1175/jcli-d-18-0577.1>
- Sun XQ, Li SL, Hong XW et al (2019b) Simulated influence of the Atlantic Multidecadal oscillation on summer Eurasian nonuniform warming since the Mid-1990s. *Adv Atmos Sci* 36:811–822. <https://doi.org/10.1007/s00376-019-8169-z>
- Tang M, Reiter ER (1984) Plateau monsoons of the Northern hemisphere: a comparison between North America and Tibet. *Mon Weather Rev* 112(4):617–637. [https://doi.org/10.1175/1520-0493\(1984\)112%3c0617:PMOTNH%3e2.0.CO;2](https://doi.org/10.1175/1520-0493(1984)112%3c0617:PMOTNH%3e2.0.CO;2)
- Trenberth KE, Fasullo JT, Shepherd TG (2015) Attribution of climate extreme events. *Nat Clim Change* 5:725–730. <https://doi.org/10.1038/nclimate2657>
- Wang H, Li DL (2019) Decadal variability in summer precipitation over eastern China and its response to sensible heat over the Tibetan Plateau since the early 2000s. *Int J Climatol* 39(3):1604–1617. <https://doi.org/10.1002/joc.5903>
- Wang SZ, Ma YM (2011) Characteristics of land–atmosphere interaction parameters over the Tibetan Plateau. *J Hydrometeorol* 12(4):702–708. <https://doi.org/10.1175/2010JHM-1275.1>
- Wang H, Hu ZY, Li DL et al (2019) Estimation of the surface heat transfer coefficient over the east-central Tibetan Plateau using satellite remote sensing and field observation data. *Theor Appl Climatol* 138:169–183. <https://doi.org/10.1007/s00704-019-02815-x>
- Watanabe T, Yamazaki K (2014) The upper-level circulation anomaly over Central Asia and its relationship to the Asian monsoon and

- mid-latitude wave train in early summer. *Clim Dyn* 42:2477–2489. <https://doi.org/10.1007/s00382-013-1888-4>
- Wei W, Zhang RH, Wen M et al (2017) Relationship between the Asian westerly jet stream and summer rainfall over Central Asia and North China: roles of the Indian Monsoon and the South Asian High. *J Clim* 30:537–552. <https://doi.org/10.1175/JCLI-D-15-0814.1>
- Wu GX, Zhang YS (1998) Tibetan Plateau forcing and timing of south Asia monsoon and South China Sea Monsoon. *Mon Weather Rev* 126(4):913–927. [https://doi.org/10.1175/1520-0493\(1998\)126%3c0913:TPFATT%3e2.0.CO;2](https://doi.org/10.1175/1520-0493(1998)126%3c0913:TPFATT%3e2.0.CO;2)
- Wu GX, Liu YM, Liu P (1999) The effect of spatially on the formation and variation of subtropical high part: I scale analysis. *Acta Meteor Sin* 57(3):257–263 ((in Chinese))
- Wu GX, Liu YM, Zhang Q et al (2007) The influence of mechanical and thermal forcing by the Tibetan Plateau on Asian climate. *J Hydrometeorol* 8:770–789. <https://doi.org/10.1175/JHM609.1>
- Wu Z, Zhang H, Krause CM et al (2010) Climate change and human activities: a case study in Xinjiang, China. *Clim Change* 99:457–472. <https://doi.org/10.1007/s10584-009-9760-6>
- Wu GX, Duan AM, Liu YM et al (2015) Tibetan Plateau climate dynamics: recent research progress and outlook. *Natl Sci Rev* 2(1):100–116. <https://doi.org/10.1093/nsr/nwu045>
- Wu GX, Zhuo HF, Wang ZQ et al (2016) Two types of summertime heating over the Asian large-scale orography and excitation of potential-vorticity forcing I. Over Tibetan Plateau. *Sci China Earth Sci* 59(10):1996–2008. <https://doi.org/10.1007/s11430-016-5328-2>
- Xenarios S, Gafurov A, Schmidt Vogt D et al (2019) Climate change and adaptation of mountain societies in Central Asia: uncertainties, knowledge gaps, and data constraints. *Reg Environ Change* 19:1339–1352. <https://doi.org/10.1007/s10113-018-1384-9>
- Xiao C, Wu PL, Zhang LX et al (2016) Robust increase in extreme summer rainfall intensity during the past four decades observed in China. *Sci Rep* 6:38506. <https://doi.org/10.1038/srep38506>
- Xu TT, Shi ZG, Wang HL et al (2016) Nonstationary impact of the winter North Atlantic Oscillation and the response of mid-latitude Eurasian climate. *Theor Appl Climatol* 124:1–14. <https://doi.org/10.1007/s00704-015-1396-z>
- Xu WH, Li QX, Jones P et al (2018) A new integrated and homogenized global monthly land surface air temperature dataset for the period since 1900. *Clim Dyn* 50:2513–2536. <https://doi.org/10.1007/s00382-017-3755-1>
- Yang K, Qin J, Guo XF et al (2009) Method development for estimating sensible heat flux over the Tibetan Plateau from CMA data. *J Appl Meteorol Climatol* 48(12):2474–2486. <https://doi.org/10.1175/2009JAMC2167.1>
- Yang K, Guo X, Wu B (2011) Recent trends in surface sensible heat flux on the Tibetan Plateau. *Sci China Earth Sci* 54:19–28. <https://doi.org/10.1007/s11430-010-4036-6>
- Ye DZ, Gao YX (1979) *Meteorology of the Qinghai-Xizang (Tibet) Plateau*. Science Press, Beijing ((in Chinese))
- Ye DZ, Wu GX (1998) The role of the heat source of the Tibetan Plateau in the general circulation. *Meteorol Atmos Phys* 67:181–198. <https://doi.org/10.1007/BF01277509>
- Yeh TC (1982) Some aspects of the thermal influences of the Qinghai-Tibetan Plateau on the atmospheric circulation. *Arch Met Geoph Biocl A* 31:205–220. <https://doi.org/10.1007/BF02258032>
- Yin ZY, Wang HL, Liu XD (2014) A comparative study on precipitation climatology and interannual variability in subtropical East Asia and Central Asia. *J Clim* 27:7830–7848. <https://doi.org/10.1175/JCLI-D-14-00052.1>
- You QL, Kang SC, Aguilar E et al (2011) Changes in daily climate extremes in China and their connection to the large scale atmospheric circulation during 1961–2003. *Clim Dyn* 36:2399–2417. <https://doi.org/10.1007/s00382-009-0735-0>
- Yu Y, Pi Y, Yu X et al (2019) Climate change, water resources and sustainable development in the arid and semi-arid lands of Central Asia in the past 30 years. *J Arid Land* 11(1):1–14. <https://doi.org/10.1007/s40333-018-0073-3>
- Yu W, Liu YM, Yang XQ et al (2021) Impact of North Atlantic SST and Tibetan Plateau forcing on seasonal transition of springtime South Asian monsoon circulation. *Clim Dyn* 56:559–579. <https://doi.org/10.1007/s00382-020-05491-0>
- Yun X, Huang BY, Cheng JY et al (2019) A new merge of global surface temperature datasets since the start of 20th century. *Earth Syst Sci Data* 11:1629–1643. <https://doi.org/10.5194/essd-11-1629-2019>
- Zhai PM, Zhang XB, Wan H et al (2005) Trends in total precipitation and frequency of daily precipitation extremes over China. *J Clim* 18:1096–1108. <https://doi.org/10.1175/JCLI-3318.1>
- Zhang C, Lu DS, Chen X et al (2016) The spatiotemporal patterns of vegetation coverage and biomass of the temperate deserts in central Asia and their relationships with climate controls. *Remote Sens Environ* 175:271–281. <https://doi.org/10.1016/j.rse.2016.01.002>
- Zhang HX, Li WP, Li WJ (2019a) Influence of late springtime surface sensible heat flux anomalies over the Tibetan and Iranian Plateaus on the LOCATION of the South Asian high in early summer. *Adv Atmos Sci* 36:93–103. <https://doi.org/10.1007/s00376-018-7296-2>
- Zhang M, Chen YN, Shen YJ et al (2019b) Tracking climate change in Central Asia through temperature and precipitation extremes. *J Geogr Sci* 29:3–28. <https://doi.org/10.1007/s11442-019-1581-6>
- Zhang J, Ma QR, Chen HS et al (2021) Increasing warm-season precipitation in Asian drylands and response to reducing spring snow cover over the Tibetan Plateau. *J Clim* 34(8):3129–3144. <https://doi.org/10.1175/JCLI-D-20-0479.1>
- Zhao P, Chen LX (2000) Study on climatic features of surface turbulent heat exchange coefficients and surface thermal sources over the Qinghai-Xizang Plateau. *Acta Meteorol Sin* 14(1):13–29
- Zhao Y, Wang M, Huang A et al (2014) Relationships between the West Asian subtropical westerly jet and summer precipitation in northern Xinjiang. *Theor Appl Climatol* 116:403–411. <https://doi.org/10.1007/s00704-013-0948-3>
- Zhao Y, Duan A, Wu G (2018) Interannual variability of late-spring circulation and diabatic heating over the Tibetan Plateau associated with Indian ocean forcing. *Adv Atmos Sci* 35:927–941. <https://doi.org/10.1007/s00376-018-7217-4>
- Zhou XJ, Zhao P, Chen JM et al (2009) Impacts of thermodynamic processes over the Tibetan Plateau on the Northern Hemispheric climate. *Sci China Earth Sci* 52:1679–1693. <https://doi.org/10.1007/s11430-009-0194-9>
- Zhu ZC, Bi J, Pan YZ et al (2013) Global data sets of vegetation leaf area index (LAI)3g and fraction of photo synthetically active radiation (FPAR)3g derived from global inventory modeling and mapping studies (GIMMS) normalized difference vegetation index (NDVI3g) for the period 1981 to 2011. *Remote Sens* 5(2):927–948. <https://doi.org/10.3390/rs5020927>
- Zhu LH, Huang G, Fan GZ et al (2017) Evolution of surface sensible heat over the Tibetan Plateau under the recent global warming hiatus. *Adv Atmos Sci* 34(10):1249–1262. <https://doi.org/10.1007/s00376-017-6298-9>
- Zhu X, Wei ZG, Dong WJ et al (2020) Dynamical downscaling simulation and projection for mean and extreme temperature and precipitation over central Asia. *Clim Dyn* 54:3279–3306. <https://doi.org/10.1007/s00382-020-05170-0>